• The knotty structure is attributed to MHD instabilities in dynamic outflows, with **entrainment** of external material as the jet propagates outward. Radio images on the kpc scale indicate that the jet structure may consist of a fast moving central column or **spine** of low plasma density, surrounded by a slower-moving (but still relativistic), denser **sheath** that captures the entrainment. Shocks may develop at the spine-sheath interface, and may seed acceleration of electrons to relativistic energies.

**Plot:** Relativistic Hydrodynamic Jet Simulations

∗ The magnetic field morphology in jets is not precisely known, but may be quasi-helical as opposed to sheet-like in character.

## 3.1 Superluminal Motion and Doppler Boosting

• Imaging over time of the jets reveals that the knots are moving outwards (the same is seen in galactic superluminal jet sources or **microquasars**), and with **apparent superluminal motion** $v_{\rm app} > c$ in the sky. **C & O, pp. 1125–8**

**Plot:** Superluminal Motion in 3C 273 and GRS 1915+105

This deception is a geometrical projection effect on the sky (flashlight+wall analogy), and has no physical basis that contradicts Einstein's theory of special relativity.

• Consider two photons reaching Earth from a jet that are observed at times $t_1$ and $t_2$. The propagation equations are

$$t_1 \;=\; \frac{d}{c} \;\;, \quad t_2 \;=\; t_e + \frac{d - v t_e \cos\phi}{c} \;, \quad (6)$$

where $t_e$ is the time delay at the source for the emission of the second photon, and we define $\Delta t = t_2 - t_1$ to be the arrival time difference.

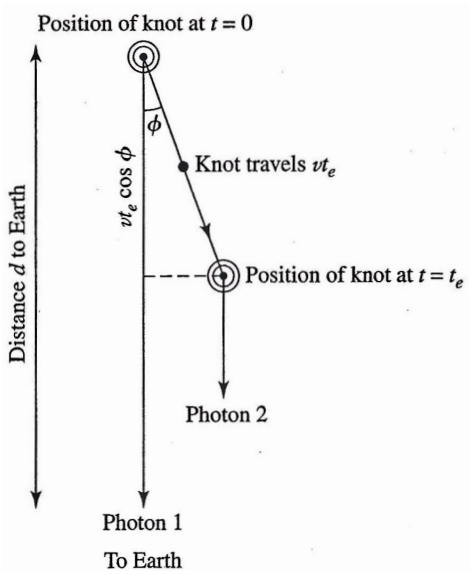


Figure 1: Superluminal motion geometry for two knots.

Then the apparent speed $v_{\rm app}$ of the knot can be coupled to the time delay via

$$\frac{v_{\rm app}}{c} \;=\; \frac{v t_e \sin\phi}{c\Delta t} \;=\; \frac{(v/c)\sin\phi}{1-(v/c)\cos\phi} \;\;, \quad \Delta t \;=\; t_e\Big(1 - \frac{v}{c}\cos\phi\Big) \;\;. \quad (7)$$

When $\phi \ll 1$ and $v \sim c$ this can yield $v_{\rm app} \gg c$! Specifically, in this domain,

$$\frac{v_{\rm app}}{c} \;\approx\; \frac{2\phi}{\phi^2 + 1/\Gamma^2} \quad \text{with} \quad \Gamma \;=\; \frac{1}{\sqrt{1 - v^2/c^2}} \;\;. \quad (8)$$

If $\phi$ is known (*difficult to measure*), this relation can be inverted to infer the relativistic speed $v$. Generally, bulk motions with $\Gamma = 1/\sqrt{1 - v^2/c^2} \sim 5 - 100$ are determined for extragalactic radio jets. Lower values are inferred for microquasars (with solar mass black holes as their central engines), and higher values for gamma-ray bursts.

# Superluminal Motion in Jets

3C 279

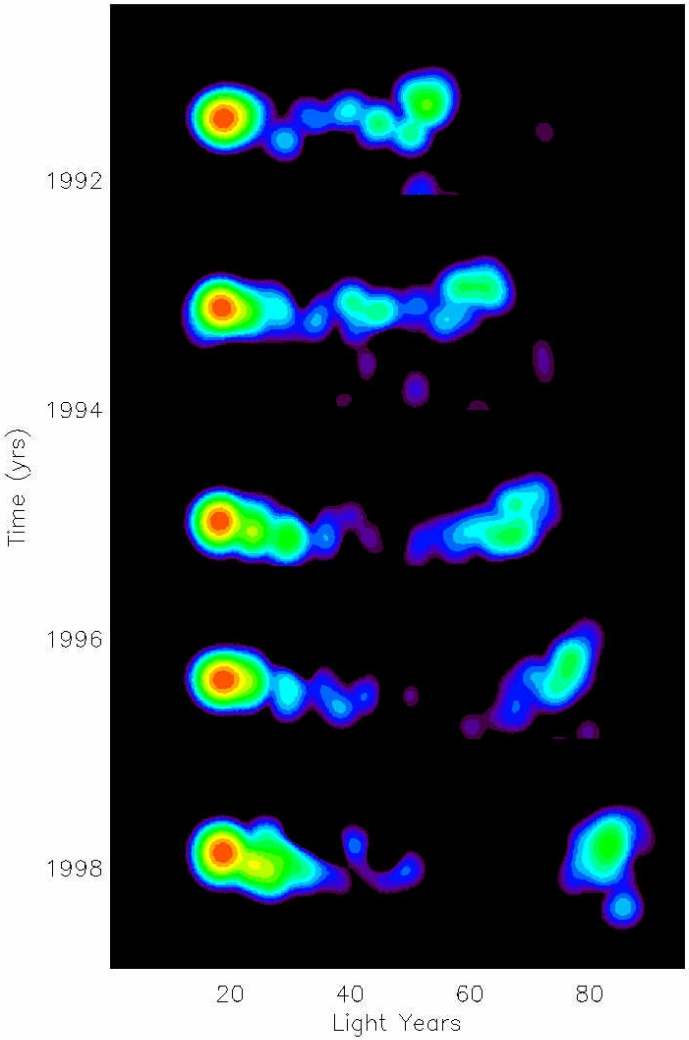


GRS 1915+105

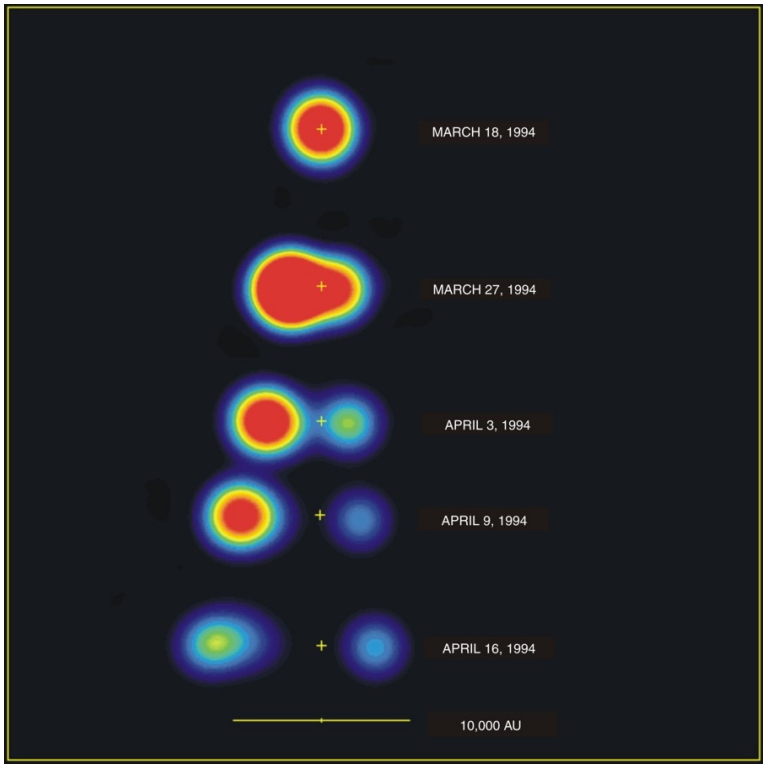


- *Left*: Time-lapse VLBI images of quasar 3C 279 depicting evolving knot positions in a superluminal motion (from Wehrle et al. 2001, ApJ 133, 297);
- See NRAO gallery *http://images.nrao.edu/387*, image courtesy of NRAO/AUI.
- *Right*: VLA Time-lapse for galactic superluminal jet in black hole candidate GRS 1915+105 (adapted from Mirabel & Rodriguez 1994, Nature **371**, 46).

• At the same time, such relativistic motions induce an enhancement of the flux from radio jets. Relative to the intrinsic comoving jet luminosity, $L_{\rm int}$, the apparent luminosity is **Doppler boosted** according to

$$L_{\rm app} \;=\; \mathcal{D}^4\, L_{\rm int} \quad , \quad \mathcal{D} \;=\; \frac{1}{\Gamma\big[1-(v/c)\cos\theta\big]} \quad , \tag{9}$$

for an angle $\theta$ $(\approx \phi)$ between the line of sight and the bulk motion vector. Here $\mathcal{D}$ is called the **Doppler factor** of the luminosity boosting.

$*$ The breakdown of this formula is that relativistic solid angle collimation (through aberration of light) contributes two powers of $\mathcal{D}$, frequency blueshifting one power, and time dilation gives another power of $\mathcal{D}$.

The sign of $\cos\theta$ clearly proves critical, and leads to the jets **beamed** towards us being much more luminous than those beamed away from the observer. Hence, jets should overwhelmingly be **one-sided**, as is observed.

• N.B. If $\Gamma \gg 1$ and $\theta \approx 0$, then small changes in $\theta$ can yield large changes in $\mathcal{D}$ and hence the apparent luminosity; this is the situation for **blazars**. This can be seen from the approximate behavior

$$\mathcal{D} \;\approx\; \frac{2\Gamma}{1+\Gamma^2\theta^2} \quad \text{for} \quad \theta \;\lesssim\; \frac{2}{\Gamma} \quad , \tag{10}$$

for which the sensitivity to $\theta$ is clearly manifested for viewing directions within the **Lorentz cone** of half-angle $\theta \lesssim 1/\Gamma \ll 1$.

## 3.2 Shock Acceleration

• Inferences of relativistic electrons in jets require a process of acceleration. The observed turbulent structure of jets, coupled with eddying/turbulence in MHD jet simulations suggests that **shocks** are present in jets.

• Formation of shocks requires only the existence of a supersonic flow impacting on a subsonic one. This affords the opportunity for **diffusive shock acceleration** (ubiquitous in astrophysics) to be active.

**Plot:** Fermi Acceleration at Shocks: Schematic

# Monte Carlo Simulation of Fermi Acceleration

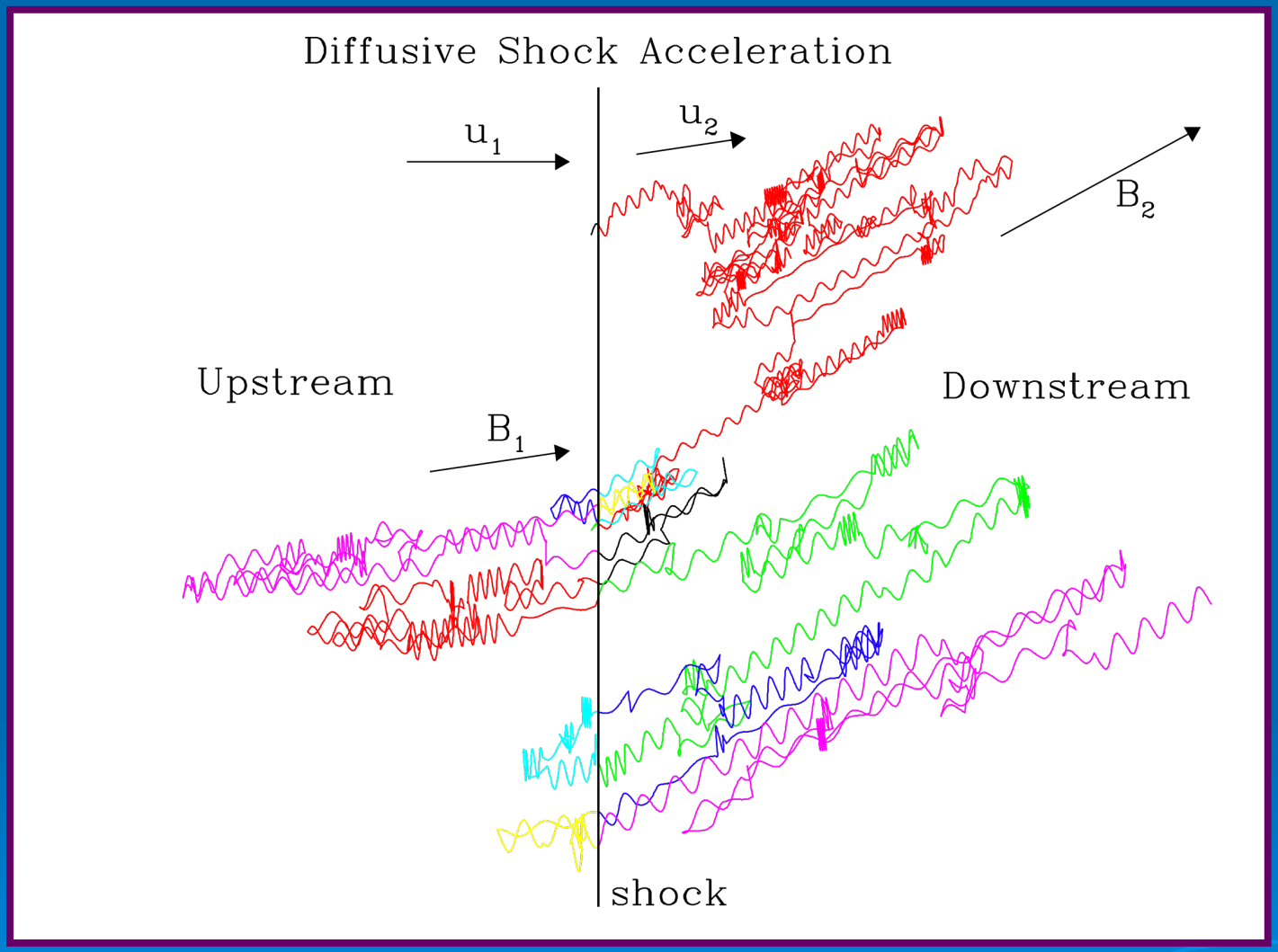


- Gyration in B-fields and diffusive transport modeled by a Monte Carlo technique; color-coded in Figure according to fluid frame energy.
- Shock crossings produce net energy gains (evident in the increase of gyroradii) according to principle of first-order Fermi mechanism.

• Such diffusive acceleration, originally posited by Fermi in 1949, is widely invoked in sources such as supernova remnants, heliospheric shocks, gamma-ray bursts, intracluster gas shocks, etc., as the site for energization of non-thermal electrons and ions.

∗ Direct evidence for the action of shock acceleration is found by particle measurements at the Earth's bow shock, other planetary bow shocks, and interplanetary traveling shocks.

• In large systems, diffusive acceleration at shocks is scale-free for significant ranges of momenta, thereby generating **power-law distributions** that are seen in the **cosmic ray** spectrum, and also can be inferred from many non-thermal astronomical sources, such as blazars and radio galaxies.

**Plot:** The Cosmic Ray Spectrum

The power-law distribution arises because the competition between energy gains in transiting the shock and convective losses from the shock environs possesses no momentum scale. For non-relativistic shocks, the power-law index $\sigma$ is universal, and depends only on the velocity compression ratio $r$:

$$\frac{dn}{dp} \propto p^{-\sigma} \quad , \quad \sigma = \frac{r+2}{r-1} \quad \text{for} \quad r \equiv \frac{u_{\rm ups}}{u_{\rm down}} \quad . \tag{11}$$

Such universality of $\sigma$ does not hold for relativistic shocks.

• Since diffusive shock acceleration in turbulent MHD plasmas avails itself of charged particle interactions with plasma wave turbulence, it is usually most efficient for **gyroresonant** wave-particle interactions. This then establishes a natural timescale for the acceleration process, namely the **gyroperiod** or inverse gyrofrequency (cyclotron frequency; $B$ in Gauss):

$$t_{\rm cyc} = \frac{1}{\omega_{\rm B}} \equiv \frac{m_e c}{eB} = \frac{5.7 \times 10^{-8}}{B} \ {\rm sec.} \tag{12}$$

Since the acceleration to electron Lorentz factor $\gamma_e$ is just time-dilated, i.e. $t_{\rm acc} \sim \gamma_e t_{\rm cyc}$ $(= \gamma_e / \dot\gamma_e)$, the energy gain rate can be written

$$\frac{dE_e}{dt} \sim 3 \times 10^7 B \ \ {\rm GeV/sec} \quad . \tag{13}$$

Hence, an AGN flare that varies on timescales around 1 hour can generate $E_{\rm max} \sim 10^{11}\,{\rm GeV} = 10^{20}\,{\rm eV}$ for typical magnetic field strengths, $B \sim 10^3\,{\rm G}$. This promotes the possibility that AGN jets can generate **ultra-high energy cosmic rays**, those with energies $E > 10^{18}\,{\rm eV}$.

# Ultra-High Energy Cosmic Rays

**Cosmic Ray Spectra of Various Experiments**

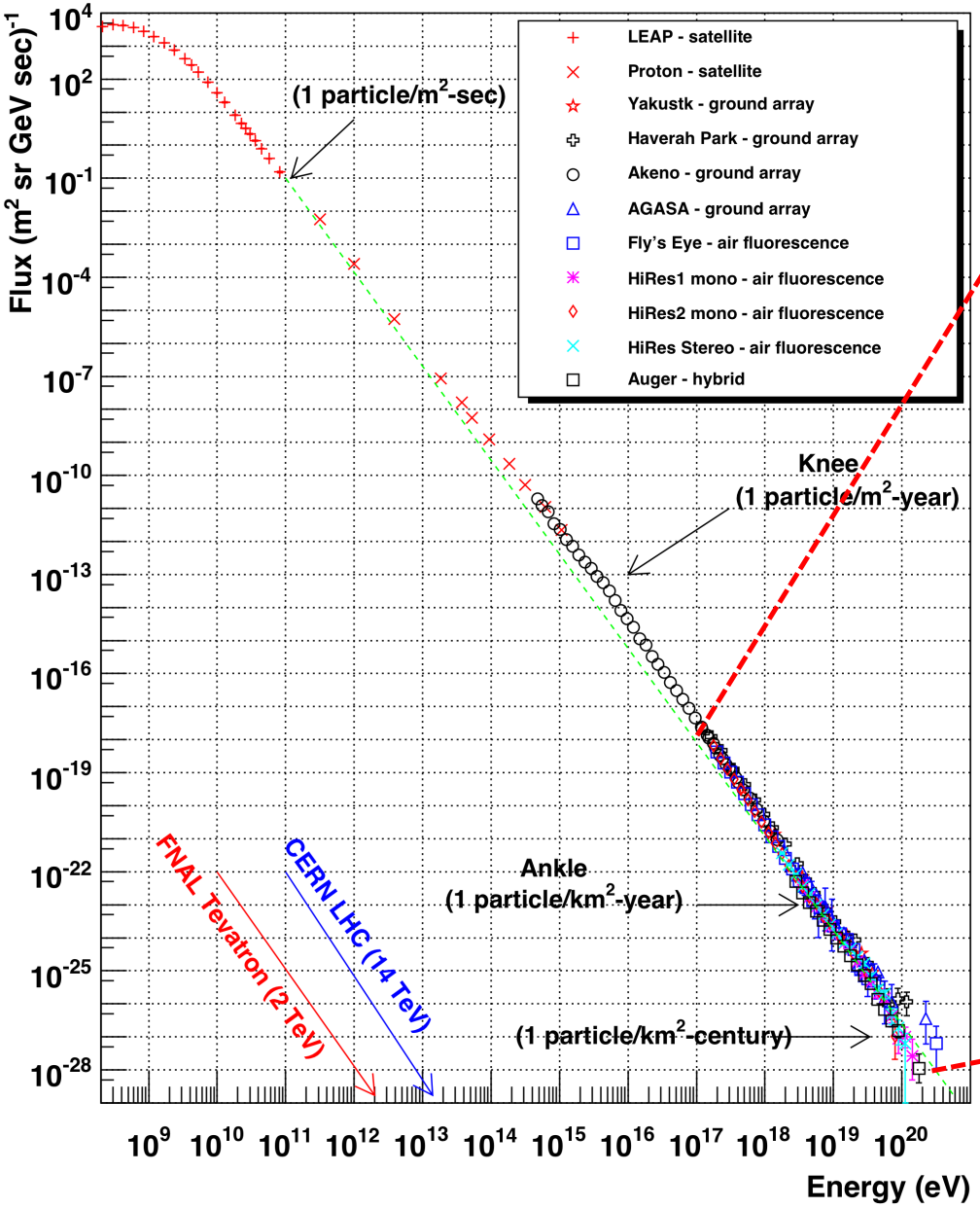


**Cosmic Ray Spectra of Various Experiments**

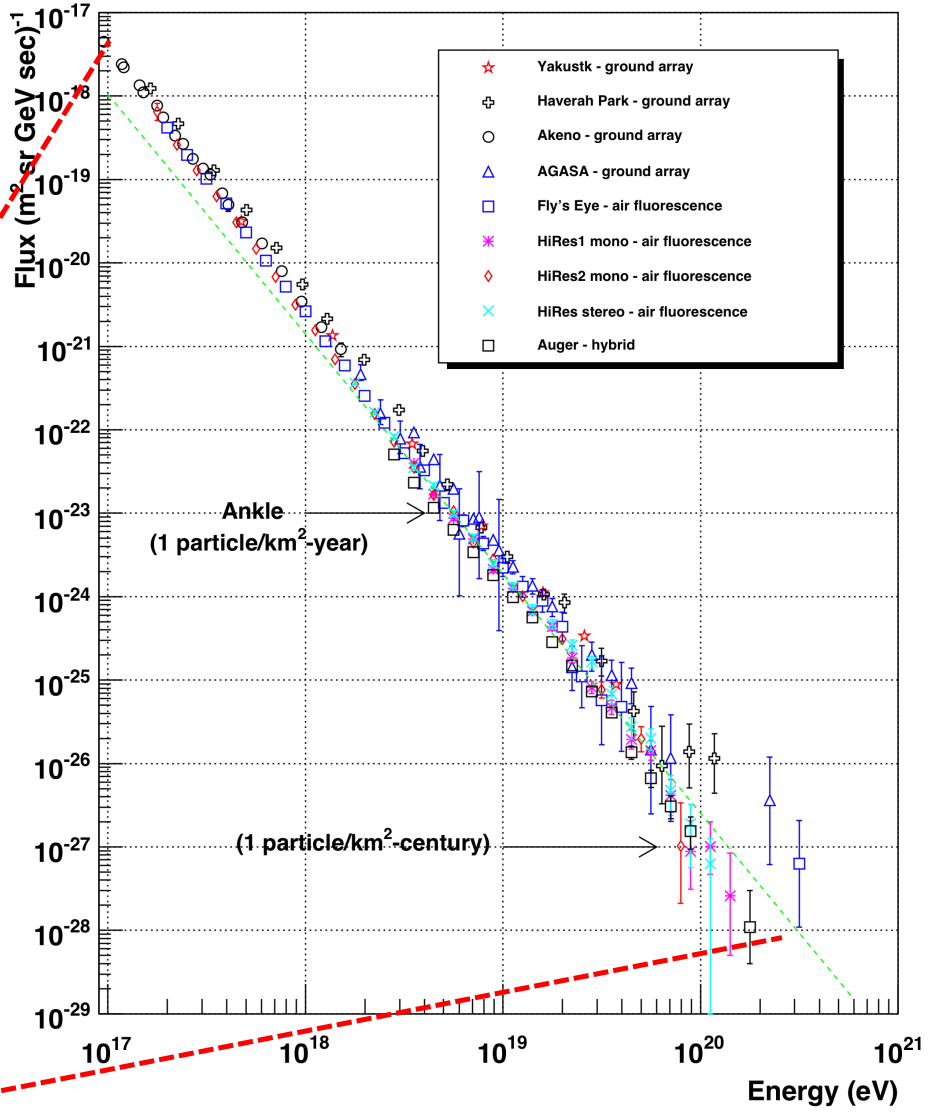


- Adapted from Simon Swordy plots by Hanlon. E>$10^{14}$eV measurements require large collecting area => air shower arrays.

## 3.3 Hot Spots in Radio Lobes

• Jets blast into the intergalactic medium (IGM), eventually dispersing in lobes (with $L_{\rm lobe} \sim 10^{44}\,{\rm erg/sec}$) which exhibit filamentary structure indicative of shocks. **Hot spots** define cores for the impact of jets on the lobe.

**C & O, pp. 1123–5**

∗ The common bending of jets shows that galaxies move through the IGM. The net mass required to bend a jet is usually only sampled on large scales, i.e., $> 100 - 200\,{\rm kpc}$.

**Plot:** Observed Bending of Extragalactic Jets

• A consideration of hot spot dynamics can provide estimates of the matter density in the jet, and the magnetic fields in lobes. In the frame of the hot spot, non-relativistic **ram pressure** can be balanced between jet and IGM contributions:

$$\rho_{\rm IGM}\, v_{\rm H}^2 \;\approx\; \rho_{\rm J}(v_{\rm J} - v_{\rm H})^2 \quad \Rightarrow \quad \frac{\rho_{\rm J}}{\rho_{\rm IGM}} \;=\; \frac{1}{(v_{\rm J}/v_{\rm H} - 1)^2} \quad . \qquad (14)$$

For $v_{\rm J} \sim c$ and $v_{\rm H} \lesssim c/30$ as a general virial estimate for the IGM flow speed (say from cluster dynamics), this establishes that $\rho_{\rm J} \lesssim 10^{-3}\rho_{\rm IGM}$. Thus, jets are quite under-dense; their key impact is that they carry a lot of momentum (and angular momentum).

**Plot:** Bow Shock Geometry for Hot Spots

• Assuming an equipartition magnetic field for $\rho_{\rm IGM} \sim 3.6 \times 10^{-25}\,{\rm g\ cm^{-3}}$ (on the low end for Galactic ISM values) then yields

$$\frac{B^2}{8\pi} \;\sim\; \rho_{\rm IGM}\, v_{\rm H}^2 \quad \Rightarrow \quad B \;\sim\; 3 \times 10^{-3}\,{\rm Gauss} \qquad (15)$$

for an estimate of the lobe's field. This is much lower than that of the field in the inner, active portions of the jet that yield their most intense emission.

∗ Note that combining this $B$ value with the approximate radius of a lobe can yield a rough estimate of the number density of non-thermal electrons via synchrotron emissivity formalism.

# Bent Jets in Radio Galaxies

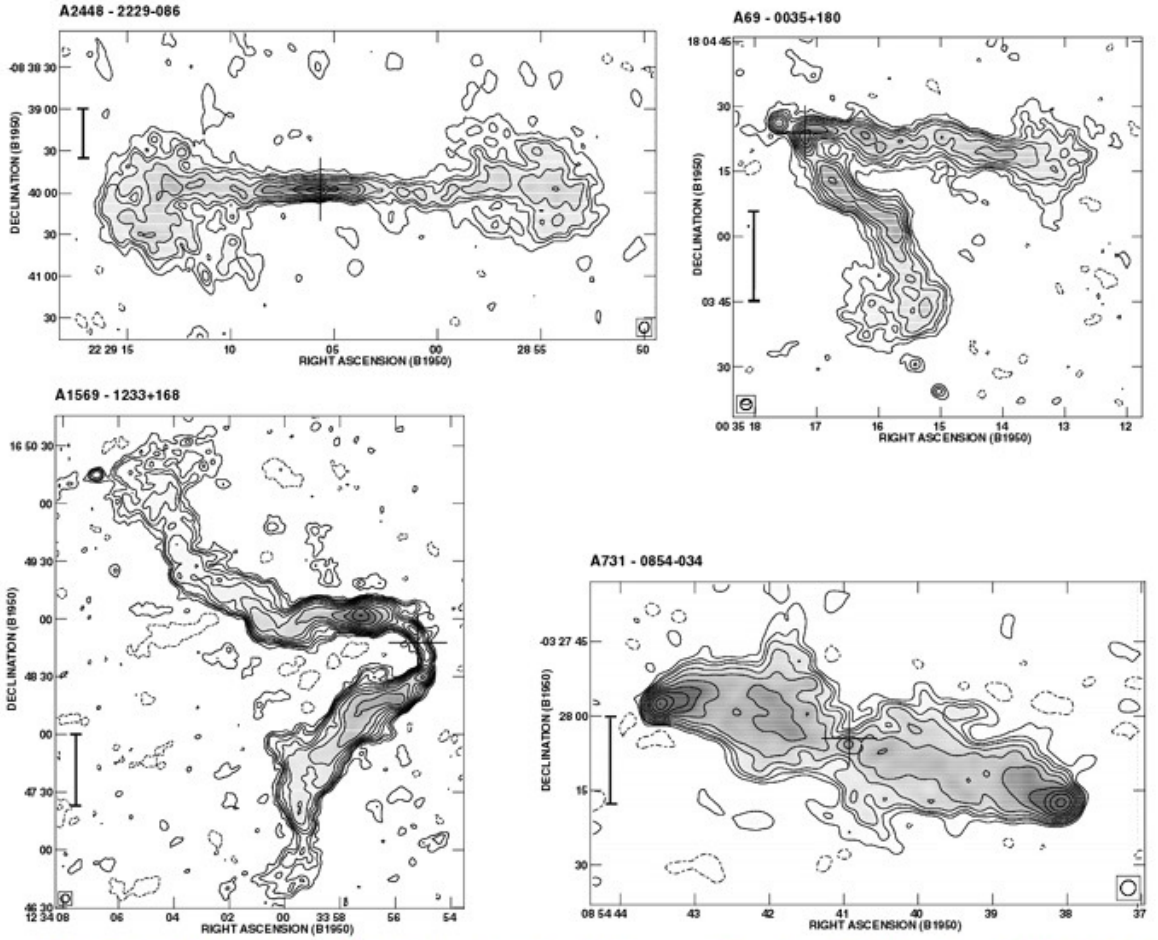


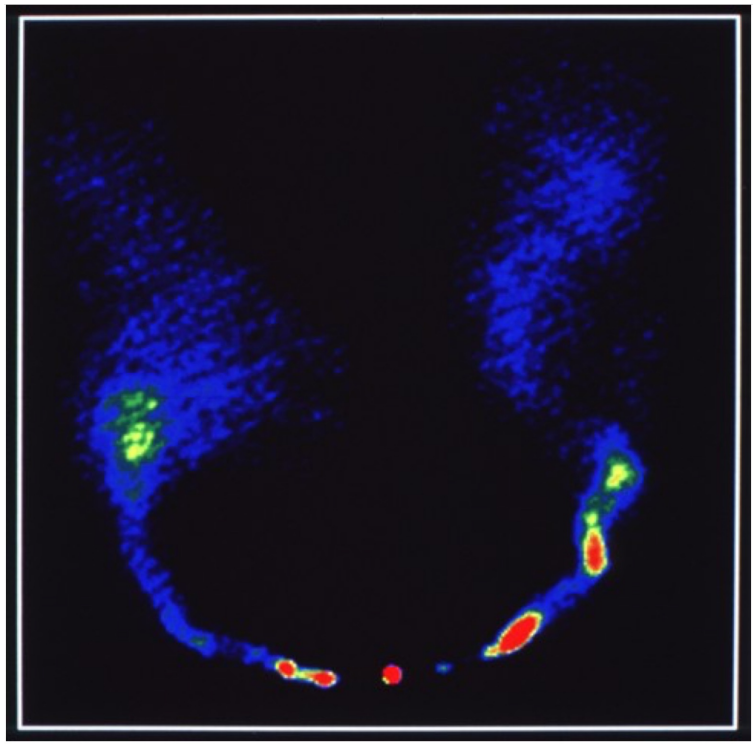

NGC 1265

- *Left*: four 20cm VLA images of radio galaxies, two with bent jets (due to M. Ledlow, from Spark & Gallagher book). *Right*: VLA image of NGC 1265 in the Perseus cluster. Courtesy: O'Dea & Owen (after original in ApJ, 1986).

# Bow Shock Geometry for Radio Lobes

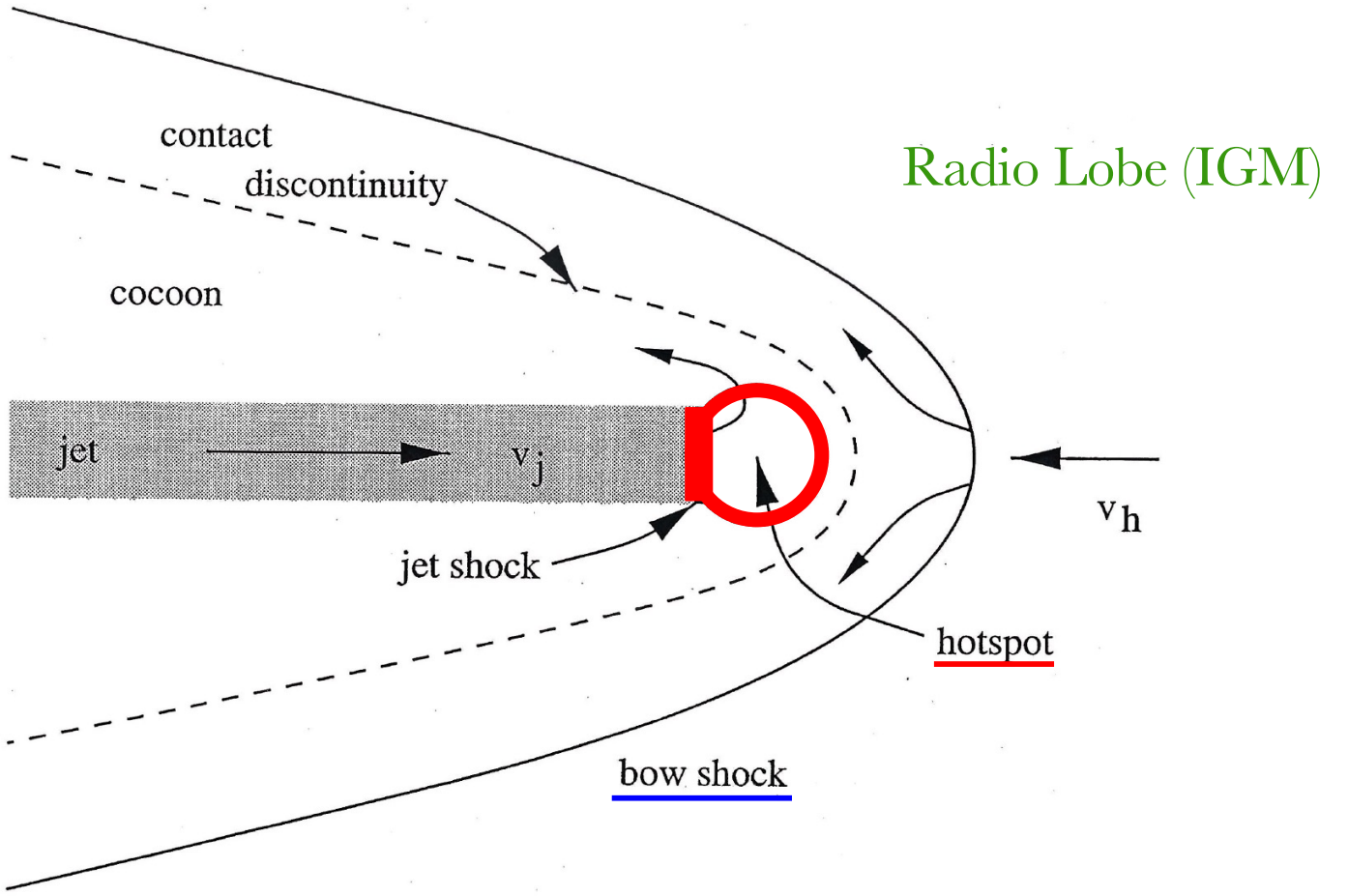


- Geometry of a jet of speed $v_j$ colliding with plasma from the IGM of speed $v_h$. The hot spot abuts the jet and is behind the bow shock.